

Hydroxyapatite/Cerium Oxide Composites: Sintering, Microstructural, Mechanical and In-vitro Bioactivity Properties

Hidroksiapatit/Seryum Oksit Kompozitleri: Sinterlenebilme, Mikroyapısal, Mekanik ve İn-vitro Biyoaktivite Özellikleri

Serdar PAZARLIOĞLU¹ 

¹Marmara University, Technology Faculty, The Department of Metallurgy and Material Science Engineering, Goztepe Campus, Istanbul/Turkey

Abstract

In the present study, the effects of cerium oxide (CeO₂) additive on the sinterability, microstructural, mechanical and in-vitro bioactivity properties of a commercially synthetic hydroxyapatite (HA) was investigated. HA without CeO₂ additive started to decompose at 1100 °C, but the decomposition temperature of the CeO₂ added samples decreased up to 900 °C. Decomposition rate of the sintered samples increased by increasing sintering temperature. It was about 5.8% for pure HA, and increased to 11.4% when the CeO₂ additive to HA reached to 2.5 wt%. SEM images showed that an excessive grain growth as well as microcracks occurred on the surface of pure HA when it was sintered at the temperatures than that of 1100 °C. The microcracks were also observed on the surface of HA-CeO₂ composites, when they were sintered at 1300 °C. The composite of HA-0.5CeO₂ sintered at 1100 °C possess the higher fracture toughness (K_{1c}) (2.510 ± 0.225 MPam^{-1/2}) and the higher compressive strength (152.73 ± 6.31 MPa) compared to other HA-CeO₂ composites, and its mechanical properties are higher than that of pure HA at about 2-3 times. In-vitro bioactivity test results showed that apatite layers on the surface of the samples were in the different morphologies.

Keywords: Hydroxyapatite, Cerium Oxide, Sintering

Öz

Bu çalışmada, seryum oksit (CeO₂) ilavesinin ticari saflıktaki bir sentetik hidroksiapatitin (HA) sinterlenebilme, mikroyapısal, mekanik ve in-vitro biyoaktivite özelliklerine etkileri incelenmiştir. CeO₂ ilavesiz HA 1100 °C sıcaklıkta dekompoze olmaya başlamış, CeO₂ ilave edilmiş numunelerde dekompoze olma sıcaklığı ise 900 °C'ye kadar düşmüştür. Sinterlenmiş numunelerin dekompoze olma oranı sinterleme sıcaklığının artmasıyla artmıştır. Saf HA'nın dekompoze olma oranı yaklaşık % 5.8 iken, HA'ya yapılan CeO₂ katkı maddesi ağırlıkça % 2.5'e ulaştığında %11.4'e yükselmiştir. SEM görüntüleri 1100 °C'nin üstündeki sıcaklıklarda sinterlenen saf HA'nın yüzeyinde aşırı tane büyümelerinin yanı sıra mikroçatlakların meydana geldiğini göstermiştir. Mikroçatlaklar ayrıca HA-CeO₂ kompozitlerinin yüzeyinde, 1300 °C sıcaklıkta sinterlendiklerinde gözlemlenmiştir. 1100 °C'de sinterlenmiş HA-0.5CeO₂ kompoziti, diğer HA-CeO₂ kompozitlerine kıyasla daha yüksek kırılma tokluğu (K_{1c}) (2.510 ± 0.225 MPam^{-1/2}) ve daha yüksek basma dayanımına (152.73 ± 6.31 MPa) sahiptir ve mekanik özellikleri saf HA'dan yaklaşık 2-3 kat daha yüksektir. İn-vitro biyoaktivite testi sonuçları, numunelerin yüzeyindeki apatit katmanlarının farklı morfolojilerde olduğunu göstermiştir.

Anahtar Kelimeler: Hidroksiapatit, Seryum oksit, Sinterleme

I. INTRODUCTION

Owing to the ageing populations worldwide, there is a strong need for developing biomaterials for tissue engineering applications. Accordingly, hydroxyapatite (HA) is considered as the most common bioceramic which can be used extensively

for repairing as well as reconstructing diseased or damaged hard tissues as a result of its excellent chemical similarity with the mineral phase of bone over other biomaterials [1]. However, the advantage of the HA chemical similarity with the mineral phase of bone is outweighed by its poor mechanical properties that prevent its bulk use in orthopedic implants. It has been investigated that load resistant HA bioceramics reinforced with other second-phase ceramic materials with moderate tolerable compressive strengths powders (for instance, zirconia, titania, magnesia or alumina) [2].

As an oxide ceramic, cerium oxide (CeO₂), is a promising material that has potential use in a number of applications such as high-temperature ceramics, catalysts, capacitor devices, UV blocking materials, oxygen sensor, fuel cells, and biodiesel production [3-6]. Apart from these applications, because of its excellent biological properties such as protection of primary cells from the detrimental effects of radiation therapy, prevention of retinal degeneration induced by intracellular peroxides and neuroprotection to spinal cord neurons, anti-inflammatory, it can be also used as a coating material and also an additive material to hydroxyapatite, which has derived from bovine femur bone [7-12]. The study about the bovine derived hydroxyapatite-cerium oxide composites has the experimental datas on the density, hardness, and compressive strength of that bioceramics, depending on the sintering temperatures as well as cerium oxide ratio. However, the effect of cerium oxide additives were not investigated on the phase stability, fracture toughness, grain growth, porosity, and in-vitro bioactivity properties of commercially available hydroxyapatite in Ref [12].

The aim of the present study was to investigate the effect of cerium oxide on a commercially available hydroxyapatite. A series of test were applied to physical and mechanical properties of sintered HA with and without cerium oxide additive. The type and amount of phases and grain size measurements were carried out using X-ray diffraction patterns and scanning electron microscope. In-vitro test were also performed to the samples having best mechanical properties.

II. EXPERIMENTAL PROCEDURE

II.1 Sample Preparation

The raw materials used in the present study were HA (Across Organics, Belgium) and CeO₂ (Sigma Aldrich, Germany) powders, and CeO₂ powder were added to HA to obtain the composites as shown in **Table 1**. The composite powders were mixed by a ball milling device at 180 rpm for 2 h. The mixed powders were uniaxially pressed to prepare the pellets according to our previous study [13]. Sintering

process was performed at 900 °C, 1000 °C, 1100 °C, 1200 °C, and 1300 °C for 4h.

Table 1. Abbreviation and composition of the samples.

Name	Abbreviation	Composition (wt/wt %)
Hydroxyapatite and cerium oxide composites	HA	HA (100)
	HA-0.5C	HA (99.5) + CeO ₂ (0.5)
	HA-1.5C	HA (98.5) + CeO ₂ (1.5)
	HA-2.5C	HA (97.5) + CeO ₂ (2.5)

II.2 Microstructural Characterization

Microstructural characterization of the samples were analyzed by a Philips X'Pert XRD machine using Cu-K α as the radiation source in the range of 2 θ values between 25° and 50°. The percentage of the phases detected by XRD analysis was determined by Rietveld analysis. The changes in the surface morphology of the sintered samples were determined by FEI Sirion XL30 SEM machine. The changes in the average grain size of the sintered samples were determined by the linear intercept method.

II.3 The Determination of Physical and Mechanical Properties

While the green and sintered densities of the samples were calculated according to **Equation 1**, the porosity ratios were calculated using **Equation 2**.

$$d = \frac{m}{v} \quad (1)$$

$$p = 100 - dr \quad (2)$$

Where; d is the green and/or sintered density (g/cm³), m is the weight (g), v is the volume (cm³), p is the porosity (%), dr is the relative density of the sintered sample.

The theoretical densities of the pelletized and sintered samples were calculated according to **Equation 3**, and the relative density values of the samples were calculated according to **Equation 4**.

$$d_t = \frac{m_t}{\left(\frac{m_1}{d_1} + \frac{m_2}{d_2}\right)} \quad (3)$$

$$d_r = \frac{d}{d_t} \times 100 \quad (4)$$

Where; d_t is the theoretical density (g/cm³), m_t is the total weight (g), m₁ is the weight of HA in mixture (g), d₁ is the theoretical density of HA (3.156 g/cm³ [14]), m₂ is the weight of CeO₂ in mixture (g), d₂ is the theoretical density of CeO₂ (7.220 g/cm³ [15]).

The shrinkage rate of the sintered samples were calculated using **Equation 5**.

$$\text{Shrinkage} = \left(\frac{L1 - L2}{L1} \right) \times 100 \quad (5)$$

Where; L1 and L2 are the lengths of green bodies and sintered bodies, respectively.

The micro (μ) – hardness of the samples was calculated using **Equation 6** by Shimadzu HMV2 microindenter at load of 200 g for 20 s. The fracture toughness (K_{Ic}) of the samples were calculated by **Equation 7** according to Ref [16] using load of 300 g for 10 s.

$$HV = 0,0018544*(P/d^2) \quad (6)$$

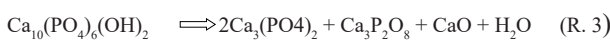
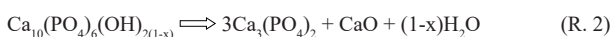
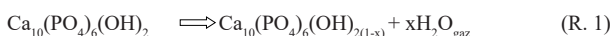
Where; HV is the vickers hardness (GPa), P is the applied load (g), and d is the diagonal indent length (mm)

$$K_{Ic} = 0.203(c/a)^{-1.5}(HV)(a)^{0.5} \quad (7)$$

Where; a is the half diagonal of the indentation (m), c is the radial crack dimension (m) measured from the center of the indent impression, and L is the crack length (m). Compression tests were done using an universal testing machine (Devotrans FU 50kN, Turkey) under a loading rate of 2 mm.min⁻¹. The in-vitro bioactivity properties of the samples, which had the higher compressive strength of HA with and without CeO₂, were determined by simulated body fluid (SBF) prepared according to Ref [17]. The apatite layers on the surface of samples immersed in SBF solutions were investigated by SEM.

III. RESULTS & DISCUSSION

Figure 1 shows the XRD patterns of pure HA. The extra peak observed at 2θ angle of 31.03 was attributed to the β -TCP, when pure HA sintered at 1100 °C, and 1200 °C. At 1300 °C, α -TCP and CaO peaks were detected in addition to HA and β -TCP phases. The XRD patterns revealed that HA powder used in the present study started to decompose at 1100 °C. **Table 2** summarizes the decomposition rates of HA to secondary phases. While pure HA started to decomposition at 1100 °C, the decomposition of CeO₂ started at dissimilar temperatures depending on additive ratios. The increase in sintering temperatures led to an increase in decomposition rates of HA-CeO₂ composites, as in pure HA. The decomposition in HA ceramics can be explained as following reactions [18]. (Ca₃(PO₄)₂)₂ is β -TCP, and Ca₃P₂O₈ is α -TCP)



Previous studies have reported that the decomposition temperatures of HA begin at different sintering temperatures between 700 °C and 1400 °C [19-24], depending on the

production process and the water vapor in the furnace atmosphere. The pure HA used in the present study started to decompose at 1100 °C. The decomposition rate of pure HA also agreed with previous reports [25-27].

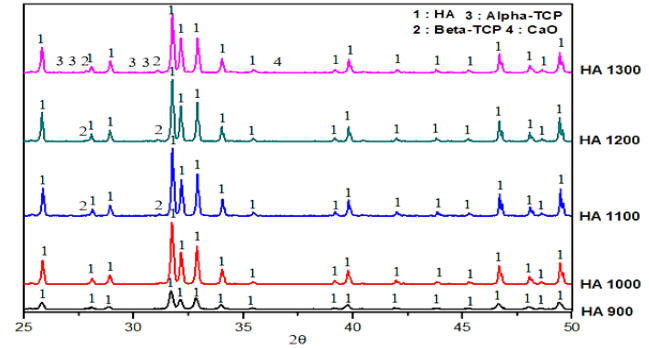


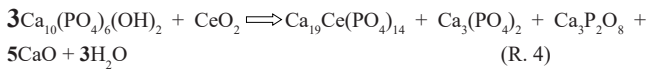
Figure 1 XRD analyzes of pure HA depending on the sintering temperatures

Table 2. The amount of HA and its decomposition rates in the sintered samples

Sample	Phase	Sintering temperature (°C)				
		900	1000	1100	1200	1300
HA	HA	100	100	97.8	96.2	94.2
	β -TCP	-	-	2.2	3.8	4.1
	α -TCP	-	-	-	-	1.6
	CaO	-	-	-	-	0.1
HA-0.5C	HA	99.2	92.5	90.5	90.6	90.2
	β -TCP	-	7.0	8.8	8.9	8.8
	α -TCP	-	-	-	-	-
	CaO	-	-	-	-	0.4
HA-1.5C	HA	98.3	92.1	90.2	89.7	87.9
	β -TCP	-	7.6	8.9	9.1	9.6
	α -TCP	-	-	-	-	1.1
	CaO	-	-	-	-	0.3
HA-2.5C	HA	96.8	91.1	89.1	88.7	86.9
	β -TCP	1.0	8.2	9.2	8.3	9.5
	α -TCP	-	-	-	0.9	1.3
	CaO	-	-	-	0.1	0.6

HA-CeO₂ composites consisted of CeO₂, Ce₇O₁₂, Ce₁₁O₂₀, Ca_{0.167}Ce_{0.7}PO₄ and Ca₁₉Ce(PO₄)₁₄ in addition to HA, β -TCP, α -TCP and CaO, as shown **Figure 2 (a)-(c)**. The CeO₂ phase detected at all sintering temperatures in the composites, regardless CeO₂ ratio, and its peak intensities at 2θ of 28.544°, and 47.479° increased as CeO₂ ratio. The Ce₇O₁₂, and Ce₁₁O₂₀ phases were only detected up to 1100 °C, which had due to the formation of oxygen vacancies in CeO₂, as stated in previous reports [28-30]. The Ca_{0.167}Ce_{0.7}PO₄ and Ca₁₉Ce(PO₄)₁₄ phases detected at dissimilar temperatures depending on the additive ratios. The Ca_{0.167}Ce_{0.7}PO₄ and Ca₁₉Ce(PO₄)₁₄ phases are formed due to the ion radii of the elements are close to each other. The ionic radii are 0.97 Å for Ce⁴⁺, 0.99 Å

for Ca²⁺, 1.07 Å for P⁵⁺, and 0.66 Å for O²⁺, respectively [31,32]. In the CeO₂ added samples, the decomposition rates increased with increase in the sintering temperatures as well as CeO₂ ratios. The decomposition of HA composited with CeO₂ at amount of 1.5 and 2.5wt % sintered at 1300 °C can be explained by Reaction 4.



The amount of HA% phase in HA-CeO₂ composites decreased to the minimum value of 86.9% at 1300 °C, as shown in Table 2. Although the addition of CeO₂ led to an increase in the decomposition rates of HA, it was found to be lower than that of previous studies. For example the amount of HA phase in a commercially available HA-SiO₂ composites decreased to the minimum value of 18.2% at 1200 °C [33], whereas it decreased to the minimum value of 57.0% for HA composited with ZrO₂ [34]. The low decomposition rate of HA-CeO₂ composites than that of the other HA based composites are due to the following reasons. 1 – The difference in sintering regime and methods. 2 – The difference in the average grain size of the raw materials. 3 – The difference in the ionic radii of the additives. The ionic radii of the Si is 0.40 Å [35], Zr⁴⁺ is 0.84 Å [36].

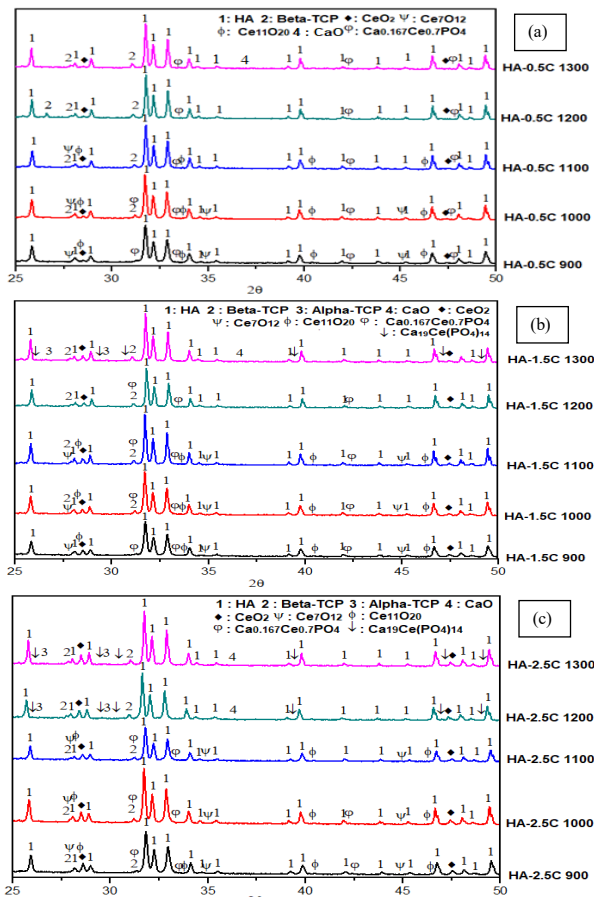


Figure 2. XRD analysis of (a) HA-0.5CeO₂, (a) HA-1.5CeO₂, and (a) HA-2.5CeO₂ composites

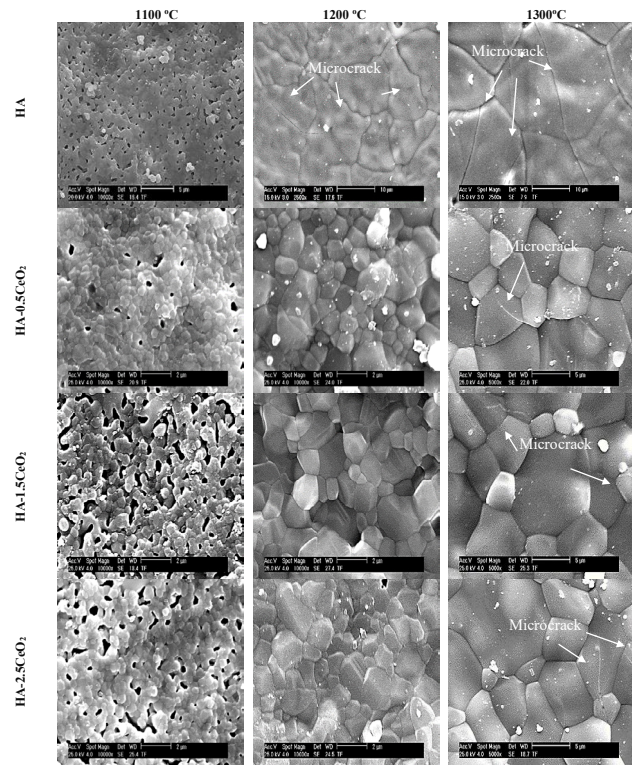


Figure 3 SEM microstructure images of samples sintered between 1100 °C and 1300 °C

Figure 3 shows the SEM images of samples sintered between 1100°C and 1300°C. As shown in Figure 3 the samples sintered at 1100 °C showed a high amount of pores that remained between the grains. These observations corresponded to the low shrinkage and the low density of sintered samples. The SEM micrographs of pure HA sintered above 1100 °C evidence a significant grain growth. For these temperatures, the average grain sizes of pure HA were measured as 7.955±1.616 μm and 17.167±2.156 μm, respectively. The microcracks on the surface of pure HA was in transgranular form. Furthermore, microcracking was also observed on the surface of pure HA. This is related to the thermal expansion anisotropy (TEA) of the HA, which leads to the generation of thermal and residual stress fields as well as it results in contraction of individual grains from neighboring grains at different rates when the pure HA ceramics sintered using conventional sintering process. If the differences in thermal contraction rates are large enough, the induced stresses can cause microcracks [37], when the grain size, G, of the HA exceeds, G_{cr}, the critical grain size [38]. As reported by Ref [39], the critical grain size is about 0.4 μm to the formation of microcracking in HA ceramics. In the present study, no microcracking observed for the pure HA at about the average grain size of 0.473 ± 0.035 μm, which is good agreement with that paper. The microcracks were also

observed to the CeO₂ added samples sintered at 1300 °C, when the grain sizes reached to $3.565 \pm 0.411 \mu\text{m}$ in HA-0.5CeO₂, $4.114 \pm 0.456 \mu\text{m}$ in HA-1.5CeO₂ and $4.283 \pm 0.541 \mu\text{m}$ in HA-2.5CeO₂, respectively. As can be seen in the results for grain size, the presence of CeO₂ inhibited the grain growth of HA particles. However, microcracks in CeO₂ added samples were found to in a shorter form than that of pure HA, and they were trapped in the grains. The microcracks on the surface of CeO₂ added samples mainly are caused

by the difference in thermal expansion coefficient (TEC) of the HA, CeO₂, β -TCP, α -TCP, CaO, Ca_{0.167}Ce_{0.7}PO₄ and Ca₁₉Ce(PO₄)₁₄ phases (HA $\approx 16.9 \times 10^{-6} \text{ }^\circ\text{C}^{-1}$ [40], CeO₂ $\approx 14 \times 10^{-6} \text{ }^\circ\text{C}^{-1}$ [41], β -TCP $\approx 14.2 \times 10^{-6} \text{ }^\circ\text{C}^{-1}$ [42], CaO $\approx 13.8 \times 10^{-6} \text{ }^\circ\text{C}^{-1}$ [43]). **Table 3** summarizes the green and relative density values of pelleted samples. It is obviously seen that the green and relative density values of the pelleted samples decreased, as the CeO₂ ratio increase. This may be related to the harder structure of CeO₂ than that of HA.

Table 3. The green and relative density values of pelleted samples

Sample ID	Theoretical density (g/cm ³)	Green density (g/cm ³)	Relative density of green bodies (%)
HA	3.156	1.651±0.016	52.316±0.529
HA-0.5CeO ₂	3.165	1.606±0.054	50.755±1.723
HA-1.5CeO ₂	3.184	1.596±0.071	50.133±2.257
HA-2.5CeO ₂	3.203	1.577±0.064	49.258±2.006

Table 4. The physical properties of HA with and without CeO₂ additive, depending on the sintering temperatures

Property	T(°C)	HA	HA-0.5CeO ₂	HA-1.5CeO ₂	HA-2.5CeO ₂
Shrinkage (%)	900	5.333±0.571	4.817±0.315	4.703±0.310	4.438±0.179
	1000	8.940±0.383	7.240±0.180	7.230±0.163	6.797±0.315
	1100	13.534±0.505	12.074±0.317	11.739±0.906	11.202±0.435
	1200	17.734±0.704	18.444±0.619	17.891±1.537	17.873±1.083
	1300	18.209±0.622	18.826±0.869	18.742±1.413	18.459±0.541
Porosity (%)	900	39.868±0.406	42.658±1.329	43.701±1.041	45.054±1.552
	1000	34.978±1.722	39.585±1.516	40.642±2.128	40.940±0.642
	1100	21.910±1.541	30.496±3.172	31.617±4.520	32.2.951±
	1200	6.832±0.224	6.797±1.690	7.930±1.477	9.903±3.361
	1300	6.304±0.469	3.793±0.370	7.157±1.786	8.661±1.366
Density (g/cm ³)	900	1.897±0.012	1.825±0.042	1.822±0.051	1.803±0.033
	1000	2.052±0.054	1.958±0.021	1.923±0.048	1.901±0.068
	1100	2.464±0.048	2.305±0.105	2.177±0.143	2.163±0.094
	1200	2.940±0.070	2.988±0.11	2.973±0.057	2.948±0.053
	1300	2.957±0.077	3.063±0.045	3.029±0.043	2.967±0.047
Relative density (%)	900	58.061±0.570	57.575±1.627	57.341±1.329	56.298±1.041
	1000	65.557±0.848	59.059±0.642	60.414±1.516	59.357±2.128
	1100	73.410±0.895	69.503±3.172	68.382±4.520	67.543±2.951
	1200	95.981±0.595	93.202±1.690	92.069±1.786	90.096±3.361
	1300	97.087±0.769	96.206±1.370	92.842±1.477	91.338±1.366

Table 4 shows the physical properties of the sintered samples. **Table 4** showed that little improvements in the physical properties were achieved up to 1100 °C. For the pure HA, the final shrinkage was $18.209 \pm 0.622\%$, whereas the final shrinkage was about 18.459-18.826% for CeO₂ added samples. The densities after sintering at or above 1200 °C reached to $2.940 \pm 0.071 \text{ g/cm}^3$ and $2.957 \pm 0.077 \text{ g/cm}^3$ for pure HA. However, although the grain sizes were lower, the HA-CeO₂ composites had higher densities than pure HA at these temperatures. This

can be related to the higher theoretical densities of CeO₂ (7.220 g/cm^3), CaO (3.37 g/cm^3), Ca_{0.167}Ce_{0.7}PO₄ (4.40 g/cm^3), and Ca₁₉Ce(PO₄)₁₄ (3.23 g/cm^3) phases than that of HA (3.156 g/cm^3). The relative density of pure HA was higher than the CeO₂-HA composites regardless of the sintering temperature used, which is due to the low theoretical density of HA than that of CeO₂. Taking theoretical density of HA as 3.156 g/cm^3 , the relative density of its attained to $97.087 \pm 0.769\%$ after sintering at 1300 °C, which is higher than that of the data in literature. For

example in Ref. [44] the authors claimed that relative density after sintering at 1300 °C was about 87%; contrary to authors of [45] who reported a relative density of $\approx 62-76\%$ for samples sintered at 1300 °C. The higher relative density of pure HA used in the present study could be attributed to the various reasons: First is the utilization of higher pelletizing pressure in the present study. Second is the HA used in this study decomposed to secondary phases at a lower rate than that of others. Third is the lower starting particulate size of HA powder. Fourth is the difference in the sintering regime and sintering time. As reported by Ref [46], the sintered density of the compacts increased with applied pelletizing

pressure because a comparatively rapid grain growth occurred. It is well-known that increase in the decomposition rates of HA leads to the decreasing in the final density because of the lower density values of the β -TCP (3.07 g/cm³ [47]), and α -TCP (2.86 g/cm³ [48]) phases. As reported Ref [49] that the difference in the particle sizes of the HA powders leads to the difference in the degree of packing during compaction. Even if the same pelletizing pressure applied to the HA powders derived from meleagris gallopova in our previous study [50], the difference in the degree of packing during compaction are reflected in the relative density values of the final products.

Table 5. The mechanical properties of HA with and without CeO₂ additive, depending on the sintering temperatures

Property	T (°C)	HA	HA-0.5CeO ₂	HA-1.5CeO ₂	HA-2.5CeO ₂
μ -hardness (GPa)	900	0.76±0.06	0.78±0.01	0.76±0.03	0.73±0.02
	1000	1.11±0.03	0.83±0.03	0.82±0.02	0.79±0.02
	1100	1.51±0.08	1.79±0.09	1.43±0.09	1.12±0.06
	1200	4.76±0.22	4.89±0.22	4.83±0.15	4.78±0.16
	1300	4.87±0.09	4.99±0.44	4.89±0.25	4.74±0.19
$\sigma_{\text{compressive}}$ (MPa)	900	91.00±6.80	84.41±5.34	77.58±16.50	60.54±6.61
	1000	102.00±10.20	91.99±11.89	99.10±6.47	86.92±21.18
	1100	130.00±6.22	152.73±15.58	123.06±23.76	115.86±18.21
	1200	101.00±5.01	139.08±6.31	116.32±11.62	112.36±8.28
	1300	65.00±5.59	107.04±5.98	69.71±3.43	58.76±10.14
K _{1c} (MPa m ^{1/2})	900	0.68±0.05	0.69±0.03	0.68±0.09	0.67±0.08
	1000	0.88±0.09	0.70±0.13	0.70±0.10	0.69±0.09
	1100	0.96±0.05	2.51±0.22	2.32±0.15	2.02±0.14
	1200	0.92±0.06	1.86±0.23	1.65±0.29	1.45±0.26
	1300	0.71±0.13	1.45±0.28	1.22±0.09	0.8±

Table 5 shows the mechanical properties of the sintered samples. Although the $\sigma_{\text{compressive}}$ of pure HA reached the maximum value of 130 ± 6.22 MPa at sintering temperature of 1100 °C, it decreased to 101.8 ± 5.01 and 65.6 ± 5.59 MPa, when it was sintered at 1200 °C and 1300 °C. Given the significant improvement in densification achieved at 1300 °C, the reduction in $\sigma_{\text{compressive}}$ can be attributed to the presence of microcracks, and increasing in the average grain sizes. Microcracks reduce the mechanical strength of HA ceramics, so HA ceramics containing TCP is not the proper material for surgical implants that require high mechanical strength [51]. It has been well established that a decrease in grain size increased the mechanical properties according to the Hall-Petch equation ($\sigma = \sigma_0 + kd^{-1/2}$) [52]. The maximum $\sigma_{\text{compressive}}$ value of pure HA obtained

at sintering temperature of 1100 °C increased to 152.73 ± 15.58 MPa with 0.5 CeO₂ additive. However, the $\sigma_{\text{compressive}}$ of HA-0.5CeO₂ composites decreased to 115.86 ± 18.21 MPa with increase in the amount of CeO₂ ratio at the same temperature. The $\sigma_{\text{compressive}}$ of HA-CeO₂ composites decreased with increasing temperature even if the relative densities of their reached to above 90%.

However; the maximum $\sigma_{\text{compressive}}$ value of 152.73 ± 15.58 MPa for HA-0.5CeO₂ composites obtained in the present study is higher than that of a previous study (107 MPa), at about 42% [12]. Increasing the sintering temperature from 900 °C to 1100 °C significantly improved the K_{1c} values of samples, but the more temperature caused to reduction the K_{1c} values. The peak K_{1c} value of pure HA of 0.967 ± 0.056

MPam^{1/2} is inside the range of 0.6-1.5 MPam^{1/2}, as stated Ref [18]. The maximum K_{1c} value of pure HA significantly improved to 2.510 ± 0.225 MPam^{1/2} by the CeO₂ additive at amount of 0.5 wt%. The higher K_{1c} values of HA-0.5CeO₂ composite compared to pure HA can be attributed to two major factors: (i) grain size refinement and (ii) crack bridging by CeO₂. The addition of CeO₂ to HA more than 0.5 wt% led to reduction the K_{1c} values of the composites at all temperatures. It can be explained by decreasing the decomposition ratio of the samples depending on the decreasing CeO₂ content as shown in **Table 2**. The peak value of 2.510±0.225 MPam^{1/2} measured to HA-0.5CeO₂ is also compatible with the K_{1c} value of human cortical bone (2-6 MPam^{1/2}). The samples sintered at below 1100 °C had the low μ -hardness values than 2 GPa. Increasing in the sintering temperature from 1100 °C to 1200 °C contributed to the sharply improvement in μ -hardness values and reached to at above 4.7 GPa. The lower hardness observed for the composites is associated with the lower density of the sintered bodies as depicted in **Table 4**. The hardness of ceramics is typically a function of porosity, density, relative density and average grain size [53]. The hardness increase with decreasing grain size is typically attributed to the reduced free path for dislocations in both metals and ceramics [54]. **Figure 4** shows the relationship between hardness and the porosity,

density, relative density and average grain size of sintered samples. The figure showed that hardness of the sintered samples increased with increasing density and relative density. Moreover, the decrease in porosity and average grain size of the sintered samples led to increasing the hardness.

Figure 5 shows the SEM images of pure HA and HA-0.5CeO₂ samples after SBF test. The surface morphology of the samples changed with the soaking time, and for 7 day of SBF immersion a layer consisted of dendritic apatitic structures on the materials could be observed. The dendritic apatite structures on the surface of pure HA were found to the more thickness after 15 days of waiting time. However, the dendritic apatite layer on the surface of HA-0.5CeO₂ composite changed to flake like layers at same waiting time. When the immersing time reached to 30 days, all of the surfaces of pure HA and HA-0.5CeO₂ composite were covered by apatite layers. The micrographs clearly exhibited that the apatite crystals has dissimilar morphologies on the surface samples. It is obviously seen that the apatite crystals on the surface CeO₂ added sample has a thicker and smooth without drying cracks. The same structures were also imaged in a previous study [55]. The positive effect of CeO₂ on the in-vitro bioactivity of hydroxyapatite may also related to the Ca₁₀-₁₆₇Ce_{0.7}PO₄ phase, which accelerate the increasing intracellular calcium ions (ubiquitous intracellular messenger) by

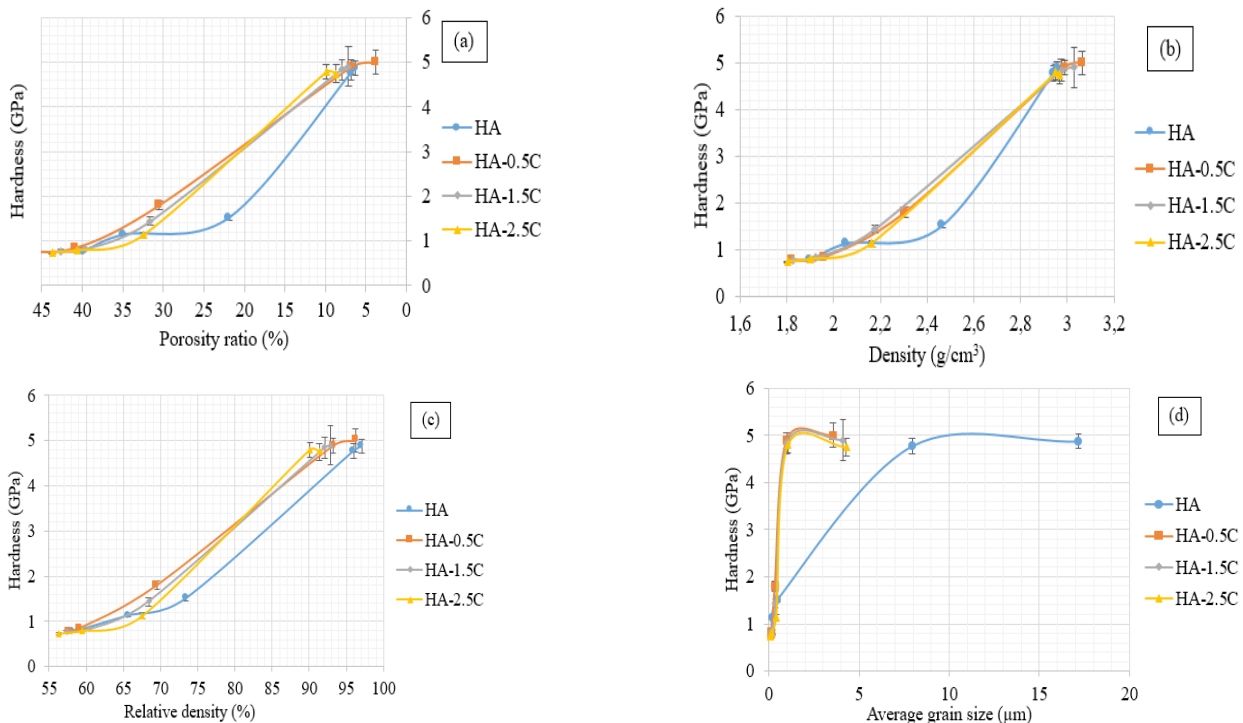


Figure 4. The relationship between microhardness and (a) the porosity, (b) the density, (c) the relative density, and (d) the average grain size of sintered samples

activation of Ca²⁺ receptor found in the membranes up-regulating signaling pathways speeding up the adhesion and proliferation of osteoblasts, as reported Ref [36]. As stated in **Table 2** that HA-0.5CeO₂ composites include β-TCP phase at amount of 8.0% in addition to HA peaks. That type combination known as biphasic calcium phosphate, which has the more bioactivity property compared to pure hydroxyapatite

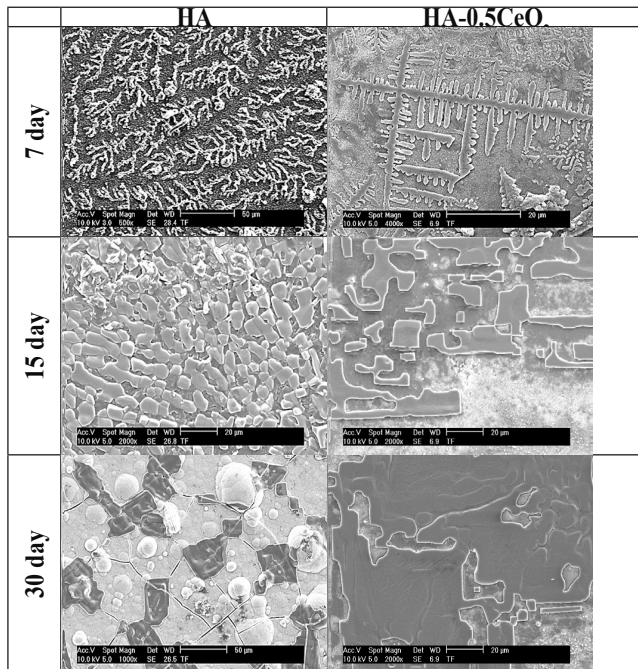


Figure 5 SEM images of pure HA and HA-0.5CeO₂ samples after SBF test

IV. CONCLUSION

In this research hydroxyapatite/CeO₂ composites were sintered at various temperature by pressureless sintering. X-ray diffraction and scanning electron microscopy results clearly revealed that the pure decomposed at 1100 °C, and when sintering temperatures at elevated temperatures an excessive grain growth with microcracks observed. By adding CeO₂ the grain growth was inhibited, but the decomposition temperature decreased to 900 °C depending on the increasing CeO₂ ratio. The mechanical properties of hydroxyapatite could be improved when it was doped with CeO₂ at amount of 0.5 wt%. The composite of HA/0.5CeO₂ can be used in human body, because it has enough fracture toughness, compressive strength and in-vitro bioactivity properties.

REFERENCES

- [1] Youness, R.A., Taha, M.A., & Ibrahim, M.A., (2017). Effect of sintering temperatures on the in vitro bioactivity, molecular structure and mechanical properties of titanium/carbonated hydroxyapatite nanobiocomposites. *J. Mol. Struct.*, 1150, 188-195.
- [2] Yetmez, M., Erkmen, Z.E., Kalkandelen, C., Ficali, A., & Oktar, F.N., (2017). Sintering effects of mullite-doping on mechanical properties of bovine hydroxyapatite. *Mater. Sci. Eng., C 77*, 470-475.
- [3] Zhou, Y., & Rahaman, M.N., (1997). Effect of redox reaction on the sintering behavior of cerium oxide. *Acta Mater.*, 45(9), 3635-3639.
- [4] Wang, X., Deng, L.L., Wang, L.Y., Dai, S.M., Xing, Z., Zhan, X.X., Lu, X.Z., Xie, S.Y., Huang, R.B., & Zheng, L.S., (2017). Cerium oxide standing out as an electron transport layer for efficient and stable perovskite solar cells processed at low temperature. *J. Mater. Chem. A*, 5, 1706-1712.
- [5] Nakane, S., Tachi, T., Yoshinaka, M., Hirota, K., & Yamaguchi, O., (1997). Characterization and sintering of reactive cerium(IV) oxide powders prepared by the hydrazine method. *J. Am. Ceram. Soc.*, 80(12), 3221-3224.
- [6] Yan, B., Zhang, Y., Chen, G., Shan, R., Ma, W., & Liu, C., (2016). The utilization of hydroxyapatite-supported CaO-CeO₂ catalyst for biodiesel production. *Energ. Convers. Manage.*, 130, 156-164.
- [7] Patil, S., Sandberg, A., Heckert, E., Self, W., & Seal, S., (2007). Protein adsorption and cellular uptake of cerium oxide nanoparticles as a function of zeta potential. *Biomater.*, 28, 4600-4607.
- [8] Hirst, S.M., Karakoti, A.S., Tyler, R.D., Sriranganathan, N., Seal, S., & Reilly, C.M., (2009). Anti-inflammatory properties of cerium oxide nanoparticles. *Small*, 5(24), 2848-2856.
- [9] Gopi, D., Murugan, N., Ramya, S., Shinyjoy, E., & Kavitha, L., (2015). Ball flower like manganese, strontium substituted hydroxyapatite/cerium oxide dual coatings on the AZ91 Mg alloy with improved bioactive and corrosion resistance properties for implant applications. *RSC Adv.*, 5, 27402-27411.
- [10] Li, K., Yu, J., Xie, Y., You, M., Huang, L., & Zheng, X., (2017). The effects of cerium oxide incorporation in calcium silicate coating on bone mesenchymal stem cell and macrophage responses. *Biol. Trace Elem. Res.*, 177, 148-158.
- [11] Ivanchenko, L.A., Pinchuk, N.D., Parkhomei, A.R., Golovkova, M.E., Molchanovskaya, M.I., & Syabro, A.N., (2009). Effect of cerium dioxide on the properties of biogenic hydroxyapatite sintered with borosilicate glass. *Powder Metall. Met. Ceram.*, 48 (5-6), 305-310.
- [12] Gunduz, O., Gode, C., Ahmad, Z., Gökçe, H., Yetmez, M., Kalkandelen, C., Sahin, Y.M., & Oktar, F.N., (2014). Preparation and evaluation of cerium oxide-bovine hydroxyapatite composites for biomedical engineering applications. *J. Mech. Behav. Biomed. Mater.*, 35, 70-76.
- [13] Pazarlioglu, S., & Salman, S., (2017). Sintering effect on the microstructural, mechanical, and in vitro bioactivity properties of a commercially synthetic hydroxyapatite. *J. Aust. Ceram. Soc.*, 53, 391-401.

- [14] Majling, J., Znáik, A., Palová, S., Stevík, S., Kovalík, D.K., & Roy, A.R., (1997). Sintering of the ultrahigh pressure densified hydroxyapatite pure xerogels. *J. Mater. Res.*, 12(1), 198-202.
- [15] Ozawa, M. (2004). Effect of oxygen release on the sintering of fine CeO₂ powder at low temperature. *Scripta Mater.*, 50, 61-64.
- [16] Pazarlioglu, S., & Salman, S., (2019). Effect of yttria on thermal stability, mechanical and in vitro bioactivity properties of hydroxyapatite/alumina composite. *J. Ceram. Process Res.*, 20(1), 99-112.
- [17] Kokubo, T., Yamamuro T., Hench L.L., & Wilson J., (1990). Handbook on Bioactive Ceramics: Bioactive Glasses and Glass-Ceramics. Vol. 1., CRC Press, Boca Raton, U.S.A. s. 1-5.
- [18] Ruys, A.J., Wei, M., Sorrell, C.C., Dickson, M.R., Brandwood, A., & Milthorpe, B.K., (1995). Sintering effects on the strength of hydroxyapatite. *Biomater.*, 16, 409-415.
- [19] Fathi, M.H., Hanifi, A., & Mortazavi, V., (2008). Preparation and bioactivity evaluation of bone-like hydroxyapatite nanopowder. *J. Mater. Process. Technol.*, 202, 536-542.
- [20] Wang, A.J., Lu, Y.P., Zhu, R.F., Li, S.T., Xiao, G.Y., Zhao, G.F., & Xu, W.H., (2008). Effect of sintering on porosity, phase, and surface morphology of spray dried hydroxyapatite microspheres. *J. Biomed. Mater. Res. A*, 87(2), 557-562.
- [21] Dorozhkin, S.V., (2008). Green chemical synthesis of calcium phosphate bioceramics. *J. Appl. Biomater. Biomech.*, 6(2), 104-109.
- [22] Mateus, A.Y.P., Barrias, C.C., Ribeiro, C., Ferraz, M.P., & Monteiro, F.J., (2008). Comparative study of nanohydroxyapatite microspheres for medical applications. *J. Biomed. Mater. Res. A*, 86(2), 483-493.
- [23] Locardi, B., Pazzaglia, V.E., Gabbi, C., & Profilo, B., (1993). Thermal behaviour of hydroxyapatite intended for medical applications. *Biomater.*, 44, 437-441.
- [24] Muralithran, G., & Ramesh, S., (2000). The effects of sintering temperature on the properties of hydroxyapatite. *Ceram. Inter.*, 26, 221-230.
- [25] Frayssinet, P., Rouquet, N., Fages, J., Durand, M., Vidalain, P.O., & Bonell, G., (1997). The influence of sintering temperature on the proliferation of fibroblastic cells in contact with HA-bioceramics. *J. Biomed. Mater. Res.*, 35, 337-347.
- [26] Fanovich, M.A., Castro, M.S., & López, J.M.P., (1998). Improvement of the microstructure and microhardness of hydroxyapatite ceramics by addition of lithium. *Mater. Lett.*, 33, 269-272.
- [27] Habibovic, P., Yuan, H., van der Valk, C.M., Meijer, G., van Blitterswijk, C.A., & de Groot, K., (2005). 3D micro environment as essential element for osteoinduction by biomaterials. *Biomater.*, 26, 3565-3575.
- [28] Hull, S., Norberg, S.T., Ahmed, I., Eriksson, S.G., Marrocchelli, D., & Madden, P.A., (2009). Oxygen vacancy ordering within anion-deficient ceria. *J. Solid State Chem.*, 182, 2815-2821.
- [29] Zinkevich, M., Djurovic, D., & Aldinger, F., (2006). Thermodynamic modelling of the cerium-oxygen system. *Solid State Ionics*, 177, 989-1001.
- [30] Kümmerle, E.A., & Heger G., (1999). The Structures of C-Ce₂O_{3+δ}, Ce₇O₁₂, and Ce₁₁O₂₀. *J. Solid State Chem.*, 147, 485-500.
- [31] Morais, D.S., Fernandes, S., Gomes, P.S., Fernandes, M.H., Sampaio, P., Ferraz, M.P., Santos, J.D., Lopes, M.A., & Hussain, N.S., (2015). Novel cerium doped glass-reinforced hydroxyapatite with antibacterial and osteoconductive properties for bone tissue regeneration. *Biomed. Mater.*, 10(5), 055008.
- [32] Gamoke, B., Neff, D., & Simons, J., (2009). Nature of PO bonds in phosphates. *J. Phys. Chem. A*, 113, 5677-5684.
- [33] Li, X.W., Yasuda, H.Y., & Umakoshi, Y., (2006). Bioactive ceramic composites sintered from hydroxyapatite and silica at 1200°C: preparation, microstructures and in vitro bone-like layer growth. *J. Mater. Sci. Mater. Med.*, 17, 573-581.
- [34] Evis, Z. (2007). Reactions in hydroxylapatite-zirconia composites, *Ceram. Inter.*, 33, 987-991.
- [35] Upasani, M. (2017). Synthesis of Y₃Al₅O₁₂:Tb & Y₃Al₅O₁₂:Tb,Si phosphor by combustion synthesis: Comparative investigations on the structural and spectral properties. *Opt. Mater.*, 64, 70-74
- [36] Mikhailov, M.M., Vlasov, V.A., Yuryev, S.A., Neshchimenko, V.V., & Shcherbina, V.V., (2015). Optical properties and radiation stability of TiO₂ powders modified by Al₂O₃, ZrO₂, SiO₂, TiO₂, ZnO, and MgO nanoparticles. *Dyes and Pigments*, 123, 72-77.
- [37] Tan, C.Y., Yaghoubi, A., Ramesh, S., Adzila, S., Purbolaksono, J., Hassan, M.A., & Kutty, M.G., (2013). Sintering and mechanical properties of MgO-doped nanocrystalline hydroxyapatite. *Ceram. Inter.*, 39, 8979-8983.
- [38] Hoepfner, T.P., & Case, E.D., (2004). An estimate of the critical grain size for microcracks induced in hydroxyapatite by thermal expansion anisotropy. *Mater. Lett.*, 58, 489 – 492.
- [39] Case, E.D., Smith, I.O., & Baumann, M.J., (2005). Microcracking and porosity in calcium phosphates and the implications for bone tissue engineering. *Mater. Sci. Eng. A*, 390, 246-254.
- [40] Miao, X., Chen, Y., Guo, H., & Khor, K.A., (2004). Spark plasma sintered hydroxyapatite-yttria stabilized zirconia composites. *Ceram. Inter.*, 30, 1793-1796.
- [41] Sameshima, S., Kawaminami, M., & Hirata, Y., (2002). Thermal expansion of rare-earth-doped ceria ceramics, *J. Ceram. Soc. Jpn.*, 110(7), 597-600.
- [42] Ruseska, G., Fidancevska, E., & Bossler, J., (2006). Mechanical and thermal-expansion characteristics of Ca₁₀(PO₄)₆(OH)₂-Ca₃(PO₄)₂ composites. *Science of Sintering*, 38, 245-253.
- [43] Chen, M., Lu, C., & Yu, J., (2007). Improvement in performance of MgO-CaO refractories by addition of nano-sized ZrO₂. *J. Eur. Ceram. Soc.*, 27, 4633-4638.

- [44] Herliansyah, M.K., Hamdi, M., Ide-Ektessabi, A., Wildan, M.W., & Toque, J.A., (2009). The influence of sintering temperature on the properties of compacted bovine hydroxyapatite. *Mater. Sci. Eng. C*, 29, 1674-1680.
- [45] Wang, P.E., & Chaki, T.K., (1993). Sintering behaviour and mechanical properties of hydroxyapatite and dicalcium phosphate. *J. Mater. Sci. Mat. Med.*, 4, 150-158.
- [46] Rootare, H.M., & Craig, R.G., (1974). Characterization of the compaction and sintering of hydroxyapatite powders by mercury porosimetry. *Powder Technol.*, 9, 199-211.
- [47] Miao, X., Chen, Y., Guo, H., & Khor, K.A., (2004). Spark plasma sintered hydroxyapatite-yttria stabilized zirconia composites. *Ceram. Inter.*, 30, 1793-1796.
- [48] Wang, X., Fan, H., Xiao, Y., & Zhang, X., (2006). Fabrication and characterization of porous hydroxyapatite/ β -tricalcium phosphate ceramics by microwave sintering. *Mater. Lett.*, 60, 455-458.
- [49] Alymov, M.I., Bakunova, N.V., Barinov, S.M., Belunik, I.A., Fomin, A.S., Ievlev, V.M., & Soldatenko, S.A., (2011). Specific features of the densification of hydroxyapatite nanopowders upon pressing. *Nanotechnologies in Russia*, 6(5-6), 353-356.
- [50] Pazarlioglu, S.S., Gokce, H., Ozyegin, L.S., & Salman, S., (2014). Effect of sintering on the microstructural and mechanical properties of meleagris gallopova hydroxyapatite. *Bio-Med. Mater. Eng.*, 24, 1751-1769.
- [51] Ryu, H.S., Youn, H.J., Hong, K.S., Chang, B.S., Lee, C.K., & Chung, S.S., (2002). An improvement in sintering property of β -tricalcium phosphate by addition of calcium pyrophosphate. *Biomater.*, 23, 909-914.
- [52] Mansour, S.F., El-dek, S.I., & Ahmed, M.K., (2017). Physico-mechanical and morphological features of zirconia substituted hydroxyapatite nano crystals. *Sci. Rep.*, 7, 43202.
- [53] Hoepfner, T.P., & Case, E.D., (2003). The influence of the microstructure on the hardness of sintered hydroxyapatite. *Ceram. Inter.*, 29, 699-706.
- [54] Wang, J., & Shaw, L.L., (2009). Nanocrystalline hydroxyapatite with simultaneous enhancements in hardness and toughness. *Biomater.*, 30, 6565-6572.
- [55] Zhu, Q., Ablikim, Z., Chen, T., Cai, Q., Xia, J., Jiang, D., & Wang, S., (2017). The preparation and characterization of HA/ β -TCP biphasic ceramics from fish bones. *Ceram. Inter.*, 43, 12213-12220.